Quaternary Science Reviews 220 (2019) 165–177

Contents lists available at ScienceDirect

Quaternary Science Reviews

journal homepage: www.elsevier.com/locate/quascirev

Millennial-scale pulsebeat of glaciation in the Southern Alps of New Zealand

Peter D. Strand [a, *], Joerg M. Schaefer [b, c], Aaron E. Putnam [a], George H. Denton [a], David J.A. Barrell [d], Tobias N.B. Koffman [a, b], Roseanne Schwartz [b]

[a] School of Earth and Climate Sciences and Climate Change Institute, University of Maine, Orono, ME 04469, USA
[b] Lamont-Doherty Earth Observatory of Columbia University, 61 Rt. 9W, Palisades, NY, 10964, USA
[c] Department of Earth and Environmental Sciences, Columbia University, New York, NY 10027, USA
[d] GNS Science, Private Bag 1930, Dunedin 9054, New Zealand

ARTICLE INFO

Article history:
Received 18 April 2019
Received in revised form
11 July 2019
Accepted 12 July 2019

Keywords:
New Zealand
Pleistocene
Cosmogenic isotopes
Glacial geomorphology
Southern Alps
Heinrich stadials
Southern Pacific
Last glacial termination

ABSTRACT

We undertook geomorphological mapping in conjunction with ^{10}Be surface-exposure dating in a previously unstudied sector of the left-lateral moraine sequence of the ice-age Pukaki glacier in the Southern Alps of New Zealand. The mapping and dating approach enabled the identification of six distinct moraine belts that were formed during maxima of glacier extent during the last glaciation. The chronology implies that ice recession occurred during Northern Hemisphere Heinrich stadials, while expansion occurred between Heinrich stadials. The ages of the moraine belts identified here are 44,000 ± 1000 yrs; 41,800 ± 1100 yrs; 36,450 ± 940 yrs 26,730 ± 740 yrs; 20,030 ± 460 yrs; and 18,000 ± 400 yrs. This moraine chronology is consistent with previous dating results from other sectors of the Pukaki moraine sequence, except that the c. 44,000 yr old moraine belt has not previously been detected elsewhere in the Pukaki moraines. Collectively with previously published ^{10}Be chronologies from the Pukaki glacier, and the adjacent Ohau glacier valley, the results demonstrate that there were several millennial-scale episodes of ice advance to full-glacial extent, and subsequent ice recession, during Marine Isotope Stages 3 and 2. This millennial-scale pulsebeat of oscillations of the Pukaki and Ohau glaciers in sympathy with the North Atlantic Heinrich episodes is further emphasized by rapid ice recession in the Southern Alps early in the last glacial termination, coeval with the onset of Heinrich stadial 1 (HS 1) in the Northern Hemisphere. That this pattern is widespread in mid-latitudes of the Southern Hemisphere is highlighted by similar chronologies of glacier variation for Andean ice lobes in the Chilean Lake District of South America.

1. Introduction

Late Quaternary glacial cycles represent the largest changes in Earth's climate over the past million years. Identifying ice-age drivers, however, remains a major problem in Earth sciences. A leading explanation involves a prominent version of the Croll (1875) and Milankovitch (1941) hypothesis, which posits that fluctuations in the volume of Northern Hemisphere ice fields and ice sheets were related to changes in mid-summer insolation intensity at 65°N latitude, due to periodic variations in Earth's orbit and consequent seasonal redistribution of incoming solar radiation. In support, Hays et al. (1976) showed that variations in global ice volume, revealed in isotopic records from Southern Ocean marine sediment cores, resemble orbitally-driven insolation patterns. However, a noteworthy implication of the Milankovitch (1941) hypothesis is that glacier volume variations should have been anti-phased between middle latitudes of the two polar hemispheres, due to the hemispherically opposed effects of orbital precession on summer insolation intensity. In contrast to this prediction, Mercer (1984) showed that the global last glacial maximum (LGM; 26,500–19,000 yrs ago, as defined by Mix et al., 2001; Clark and Mix, 2002, and Clark et al., 2009), and the last glacial termination, were broadly synchronous for the Patagonian Ice Field in the Chilean Lake District in the Andes of South America and for the Laurentide Ice Sheet in the Great Lakes region of North America.

* Corresponding author.
E-mail address: peter.strand@maine.edu (P.D. Strand).

https://doi.org/10.1016/j.quascirev.2019.07.022
0277-3791/

Existing published chronologies for the Last Glaciation moraines of two major mountain-valley glacier systems in the Southern Alps of New Zealand, the Ohau and Pukaki valleys, show that maximum glacier extent (local last glacial maximum; LLGM) was achieved prior to the global LGM, and that there were several episodes of ice advance to full-glacial extents, spanning Marine Isotope Stages (MIS) 4, 3 and 2. Those episodes coincided variously with times of high, low, or intermediate values of local summertime insolation intensity (Kelley et al., 2014; Doughty et al., 2015; Schaefer et al., 2015; Shulmeister et al., 2018, 2019). Variations of glaciers in the Southern Alps are controlled by the summer melt season and the glaciers adjust quickly to atmospheric temperature changes (Oerlemans, 1994; Anderson and Mackintosh, 2006; Anderson et al., 2010; Doughty et al., 2015; Mackintosh et al., 2017). Overall, the existing chronologic control on glacial landforms indicates that ice-age glacier fluctuations in the middle-latitudes of the Southern Hemisphere, as presumed indicators of climatic conditions, cannot be explained by local variations in summer insolation intensity alone (Mercer, 1984; Denton et al., 1999; Putnam et al., 2013a; Kelley et al., 2014; Doughty et al., 2015; Shulmeister et al., 2019).

Previous studies of the Pukaki moraine sequence indicate that older components are preserved on the left-lateral sector of the moraine system but have been overridden by younger moraines in the terminal area (Schaefer et al., 2006, 2015; Kelley et al., 2014; Doughty et al., 2015). The purpose of the present study is to document the ages of a previously uninvestigated sector of the Pukaki moraine sequence and assess the implications of the results, particularly in regard to the influence of millennial-scale climate fluctuations on moraine formation.

2. Setting

New Zealand is antipodal to the North Atlantic region and therefore is well positioned for the evaluation of hypotheses concerning climate-forcing mechanisms that coupled the polar hemispheres. Key geographic and geomorphologic elements pertinent to New Zealand study areas include the Subtropical Frontal Zone (STF Zone) which marks the equatorward fringe of the Southern Ocean and lies adjacent to the Southern Alps, and the southern westerly wind belt, which intersects the Southern Alps. The East Australian Current (EAC) and Leeuwin Current (LC) are the dominant ocean currents influencing local temperatures in the southern Australasia region (Fig. 1).

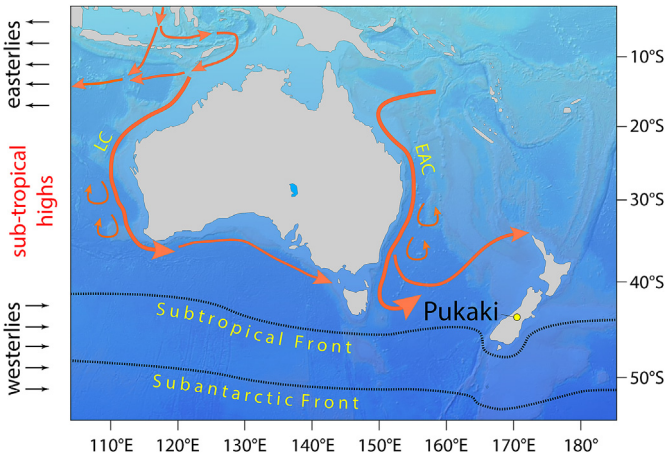

Fig. 1. Map of the southwest Pacific region. Colored arrows depict generalized ocean currents. LC: Leeuwin Current; EAC: East Australian Current (adapted from De Deckker et al., 2012 and Carter et al., 1998).

During recent glaciations, ice tongues extended out from extensive ice-fields in the Southern Alps to form local piedmonts, with post-glacial lakes such as Ohau and Pukaki occupying the lower reaches of the troughs of their former valley glaciers (Fig. 2). Extensive lateral and terminal moraine sequences lie along the flanks of many of the glacier troughs. Mesozoic-age bedrock of the eastern side of the Southern Alps for the most part comprises quartzo-feldspathic greywacke sandstone and argillite mudstone (Cox and Barrell, 2007), with the greywacke providing a valuable target for surface exposure dating. Detailed studies have been completed previously on the Pleistocene to Holocene moraine sequences of three large valleys draining the eastern side of the Southern Alps, the adjacent Ohau and Pukaki valleys and their catchments (Schaefer et al., 2006, 2009, 2015; Putnam et al., 2010a, 2013a; Kaplan et al., 2013; Kelley et al., 2014, Doughty et al., 2015) and the Rakaia valley (Fig. 2), located about 150 km to the northeast (Putnam et al., 2013b; Koffman et al., 2017).

The Pukaki catchment has a north-south orientation and originates from the highest portion of the Southern Alps. The largest modern glaciers in the Southern Alps occur in the upper reaches of the Pukaki catchment. The extensive outwash plain of the Tasman River, with valley-side tributary fans, occupies the floor of the main valley and drains to a prograding delta at the head of Lake Pukaki (Fig. 2). The lake outlet has been impounded and raised to provide storage water for hydro-electric power generation, and when full, stands almost 50 m higher than its natural level (Barrell and Read, 2014).

Well-preserved lateral and terminal moraine belts outboard of the southern, eastern, and western shores of Lake Pukaki mark the limit of the ice-age Pukaki glacier. At its fullest extent, the Pukaki glacier was ~85 km long and 1300 km^3 in area (Porter, 1975). Modeling studies suggest that a temperature depression of 6.0 – 6.5 °C was sufficient to cause the ~850 m snowline depression responsible for the maximum LGM extent of the Pukaki glacier (Golledge et al., 2012; Putnam et al., 2013a).

Vegetation cover in the Mackenzie basin has varied since the LGM. Pollen records indicate an early Holocene cover of shrub/small tree species (McGlone and Moar, 1998). From the mid-Holocene onwards, natural fires led to vegetation alternating between montane forest and open grasslands (McGlone and Moar, 1998). Since human arrival ~800 yrs ago, fires have further reduced the native vegetation cover. Mammals and rodents introduced by Europeans, including rabbits and sheep, have exacerbated soil erosion in some areas. In recent years, a halt in burning has led to the spread of introduced Northern Hemisphere conifers and recolonization of native shrubs and tussocks.

3. Glacial geology & geomorphology

Previous geological and geomorphological work relating to the Lake Pukaki area is summarized by Barrell and Read (2014). The authors note the subdivision of the Late Quaternary glacial and glacifluvial deposits of the Pukaki glacier into four geological formations, from oldest to youngest, Wolds, Balmoral, Mt John, and Tekapo, with same-named geomorphic units developed on the surfaces of the glacial and glacifluvial deposits. The latter three formed during the Last Glaciation, with Balmoral moraines (Barrell, 2014) farthest outboard of the Lake Pukaki trough and Tekapo moraines lying closest to the lake basin. The Tekapo and Mt John geomorphic units collectively encompass the global LGM at Lake Pukaki. The Balmoral moraines represent the greatest extent that the Pukaki glacier attained during the Last Glaciation and were deposited during MIS 4 (Schaefer et al., 2015) (Fig. 2).

The Pukaki glacier trough has an asymmetric cross-valley profile, with a relatively steep right-lateral (western) flank, and a

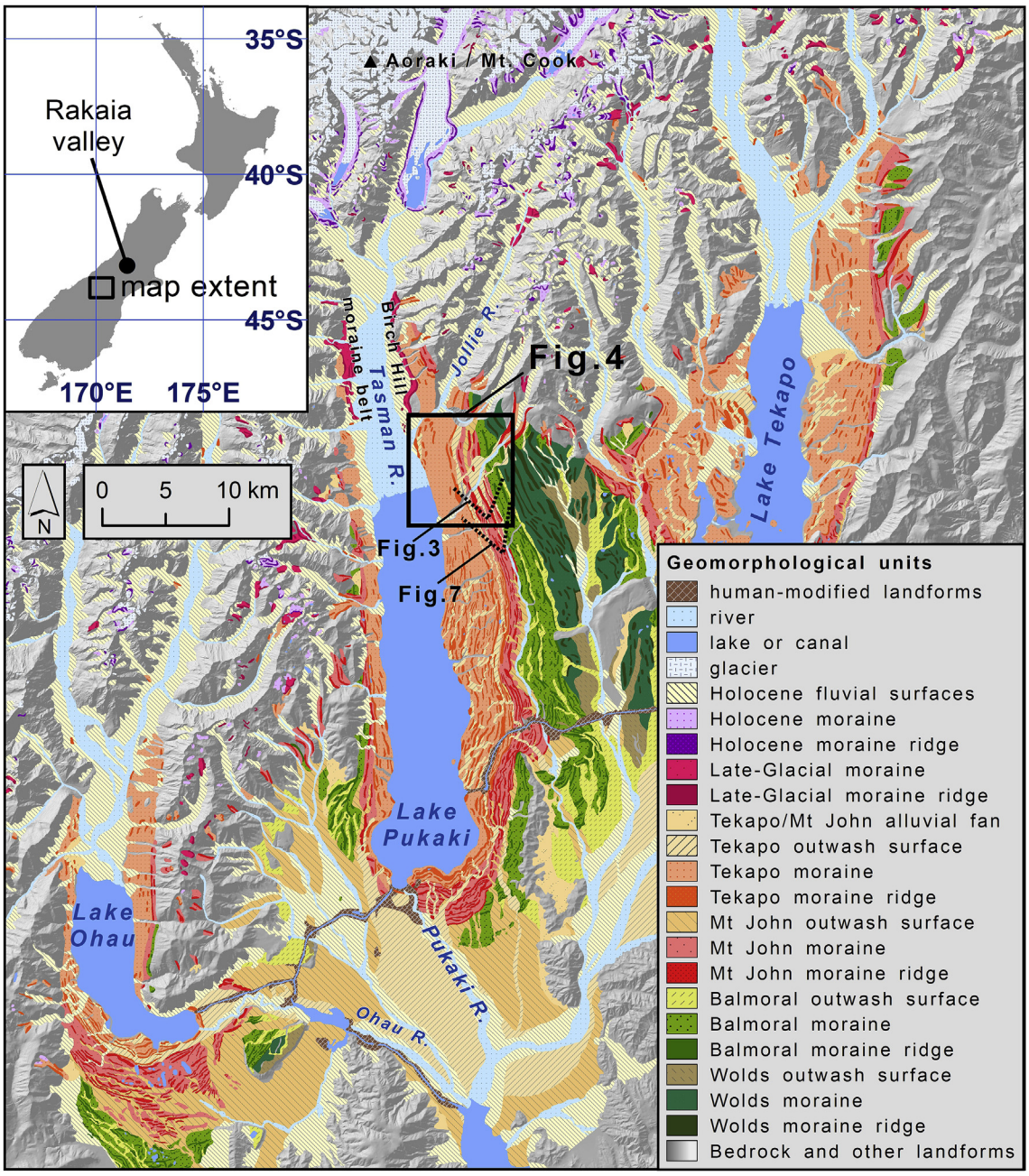

Fig. 2. Overview map of glacial geomorphology adapted from Barrell et al. (2011). Location diagram and geomorphologic unit legend are inset. Black box marks the extent of Fig. 4 map and the dotted lines denote the approximate fields of view in Figs. 3 and 7.

gentler left-lateral (eastern) flank. The left-lateral moraine belts form a geographically extensive landform feature. The northern sector of those moraines, covering an area of ~25 km^2, lying south of the Jollie River tributary valley of the Pukaki catchment, comprises the field area for this study. The Mt John and Tekapo moraine belts in this area trend north-south, paralleling the eastern shore of Lake Pukaki (Fig. 2). Up-valley, the Birch Hill moraine belt is situated about 7 km north of the present-day lake (Putnam et al., 2010a) (Fig. 2).

We mapped the moraine belts on the basis of morphology and continuity of landforms (Fig. 4). Outwash channels between moraine belts aided in differentiating the map units. We informally labelled the moraine belts, from youngest to oldest: belt 1, belt 2, belt 3, belt 4, belt 5, and belt 6 (Fig. 7). Moraine belt 1 is classified as a Tekapo landform while moraines belts 2 through 6 are Mt John (Barrell and Read, 2014). Moraine belts 1 and 2 are continuous features in the study area while belts 3 through 6 are more fragmented (Fig. 3). Outwash channels differentiate the numbered belts. Moraine belt 1 forms the innermost crest of the field area bench at the margin of a steep slope exposed during deglaciation.

4. Methods

We used the ^{10}Be surface exposure-age dating technique to determine the chronology of formation of the moraine belts. A key component in our methodology is first differentiating each moraine belt on the basis of thorough glacial geomorphologic mapping. We use cross-cutting relationships of moraine belts and outwash

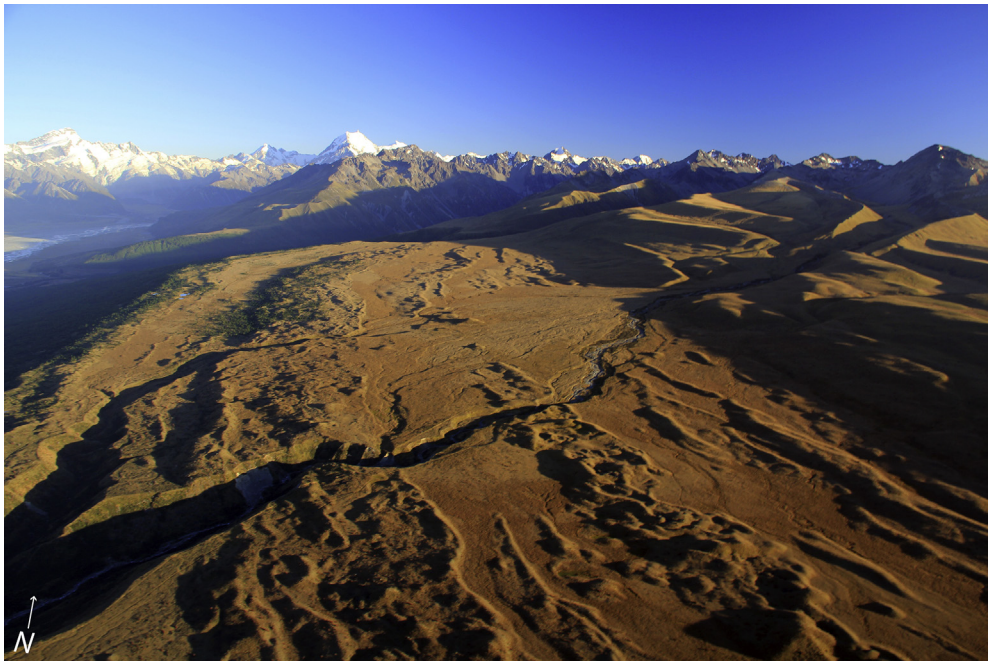

Fig. 3. Oblique aerial view looking north-northwest across the flattish bench of the study area. The Tasman River valley floor is visible to upper left, with Aoraki/Mount Cook the prominent icy peak in the background. The vantage position is indicated in Fig. 2. Photo: A.E. Putnam.

channels to delineate and identify glacial landforms. We then sampled large boulders that are well-embedded in the crests of moraine ridges, indicating little-to-no boulder movement since deposition. Boulders are predominantly hard quartzo-feldspathic greywacke sandstone, and we targeted boulders that had even, flat-topped surfaces. Boulders with steep sloping tops or fractured surfaces were avoided, as were boulders with signs of post-depositional surface erosion, such as lack of lichen cover and fresh-looking surfaces, and any showing evidence for disturbance by fluvial processes, slope movement, or human activities. We measured the dimensions of each boulder, noting its position relative to the moraine ridge on which it was deposited. Where possible, we sampled several boulders from each moraine ridge. Examples of sampled boulders are shown in Fig. 5.

Samples were collected using the "drill-and-blast" method of Kelly et al. (2008). We used a Hilti TE-6A rotary hammer drill to bore a hole into the boulder. We then placed and detonated a small charge using a 15-cm nail and hammer, in order to remove the sample from the boulder surface (Kelly et al., 2008). We measured the coordinates of each sample using a Trimble ProXH GPS instrument. The GPS measurements then were corrected differentially against data from the Mount John Observatory base station. Each sample was sketched and described. A clinometer and compass were used to document the surrounding skyline for calculation of a topographic shielding correction. Each boulder was photographed from several vantages. We also noted the presence of any quartz veins and measured their relief from the boulder surface, as well as the thickness of the surface rock weathering rind. We measured the dip angle and dip direction of each surface targeted for sampling using either the GeoID™ application on an Apple iPad or else a Brunton compass.

Samples were processed at the Lamont-Doherty Earth Observatory Cosmogenic Isotope Laboratory using the methods of Schaefer et al. (2009). The Cosmogenic Isotope Laboratory procedures include both the physical and the chemical preparation of samples, as described online at http://www.ldeo.columbia.edu/res/pi/tcn/. The CAMS accelerator at the Lawrence-Livermore National Laboratory was employed to measure the ratio of ^{10}Be to ^{9}Be. Samples were measured relative to the 07KNSTD standard (^{10}Be/^{9}Be = 2.85e^{-12}) (Nishiizumi et al., 2007). Measurements were then corrected for boron contamination and for ^{10}Be in procedural blanks, which together represent changes of ~0.5% in the ^{10}Be concentrations. Analytical uncertainties were generally ~2%. Reported sample ^{10}Be concentration uncertainties have been propagated with uncertainties in the measured blank ^{10}Be concentrations.

We calculated surface-exposure ages using the ^{10}Be production rate of Putnam et al. (2010b), together with the scaling methods of Stone (2000; 'St') and a version of the Stone (2000) scaling that incorporates a high-resolution version of the Lifton et al. (2008) geomagnetic model ('Lm'). Abbreviations follow the nomenclature of Balco et al. (2008). Calculations were carried out using a wrapper MATLAB script, modified from the CRONUS-Earth online calculator, version 2 (Balco et al., 2008), following Putnam et al. (2012; 2013a). Mean surface air pressures were derived from NCAR monthly surface station climatology and incorporated in the CRONUS calculator. A rock density of 2.7 g/cm^3 was assumed and a thickness correction applied for each sample. Following Schaefer et al. (2009, 2015) and Putnam et al. (2010b; 2013a) we did not apply a correction for snow cover. This is due to the low snow accumulation rates in the region and to the exposed nature of raised boulder tops. Erosion rates are not incorporated into the age calculations because of the resistant nature of greywacke boulder surfaces (Schaefer et al., 2006, 2009; 2015), and also because no erosion-rate correction was applied at the nearby local ^{10}Be calibration site by Putnam et al. (2010b), therefore any common erosion characteristics of boulders in our study area versus the calibration site are effectively incorporated into the production rate.

5. Results

Forty-one ^{10}Be surface-exposure ages were obtained in this study. The ages are internally consistent and afford a chronology of

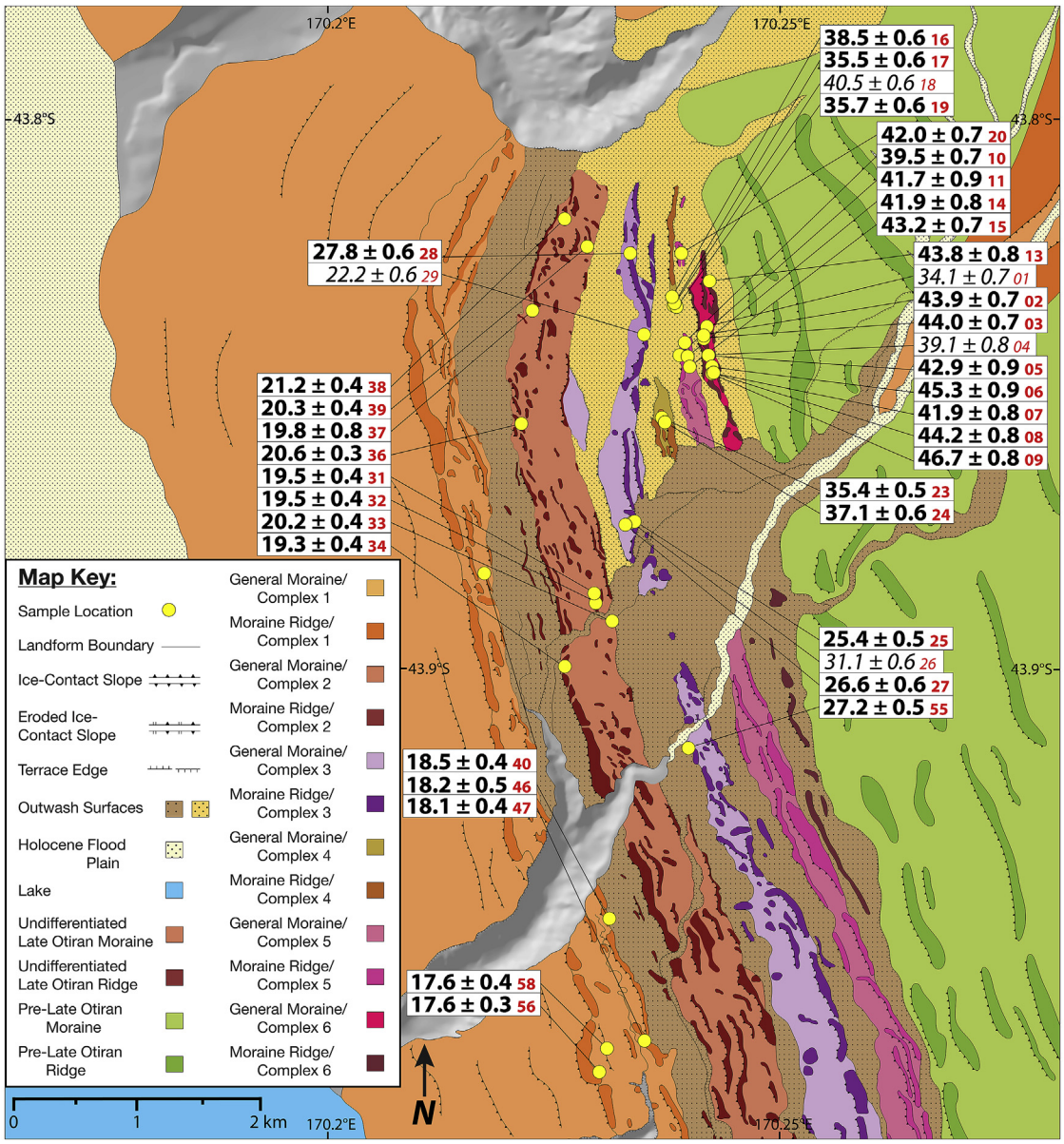

Fig. 4. Glacial geomorphic map of landforms in the field area discussed in the text. Annotations indicate ages and sample locations. Refer to Fig. 2 for map location within the Pukaki moraine system. Geomorphological symbols are described in legend, inset.

the left-lateral moraine belts deposited in the study area by the Pukaki glacier. The results from ^{10}Be sample analysis and procedural blank ^{10}Be/^{9}Be ratios are given in Table 1 and Table 2, respectively. All age calculations are referenced to calendar years before collection (i.e., before AD 2013). Hereafter, we discuss ages calculated using the Putnam et al. (2010b) calibration data set and 'Lm' scaling protocol. Uncertainties presented with individual exposure ages reflect 1σ analytical uncertainties. Samples marked by a single asterisk (*) next to the sample ID are considered outliers and are not included in the statistical analyses. Samples are determined to be outliers if they are out of morphostratigraphic order or differ from other ages from the same moraine belt in a statistically significant way. Anomalously young ages from a boulder surface can be due to post-depositional surface erosion or boulder movement, while anomalously old surface ages are most readily attributed to prior exposure to cosmogenic rays.

From the individual ages on each moraine belt, an overall age for each moraine belt was calculated. Calculated landform ages and associated statistics are given in Table 3. Landform ages are calculated using the arithmetic mean of the sample ages. Each landform age uncertainty is calculated by propagating in quadrature the standard error of the mean (SEM) and production-rate uncertainty. Here, the production-rate uncertainty is equal to 2.1%, from Putnam et al. (2010b). All ages presented in the text from this study are shown as landform age (arithmetic mean) ± landform age uncertainty (SEM and production rate uncertainty). Probability density functions (i.e. "camelplots") in Fig. 6 give visual representations of age populations of moraine belts. A summary of calculated ages is plotted in Fig. 7.

5.1. Moraine belt 6

Ten ages from moraine belt 6, the outermost and therefore oldest landform examined here, range from 34,050 ± 670 yrs to

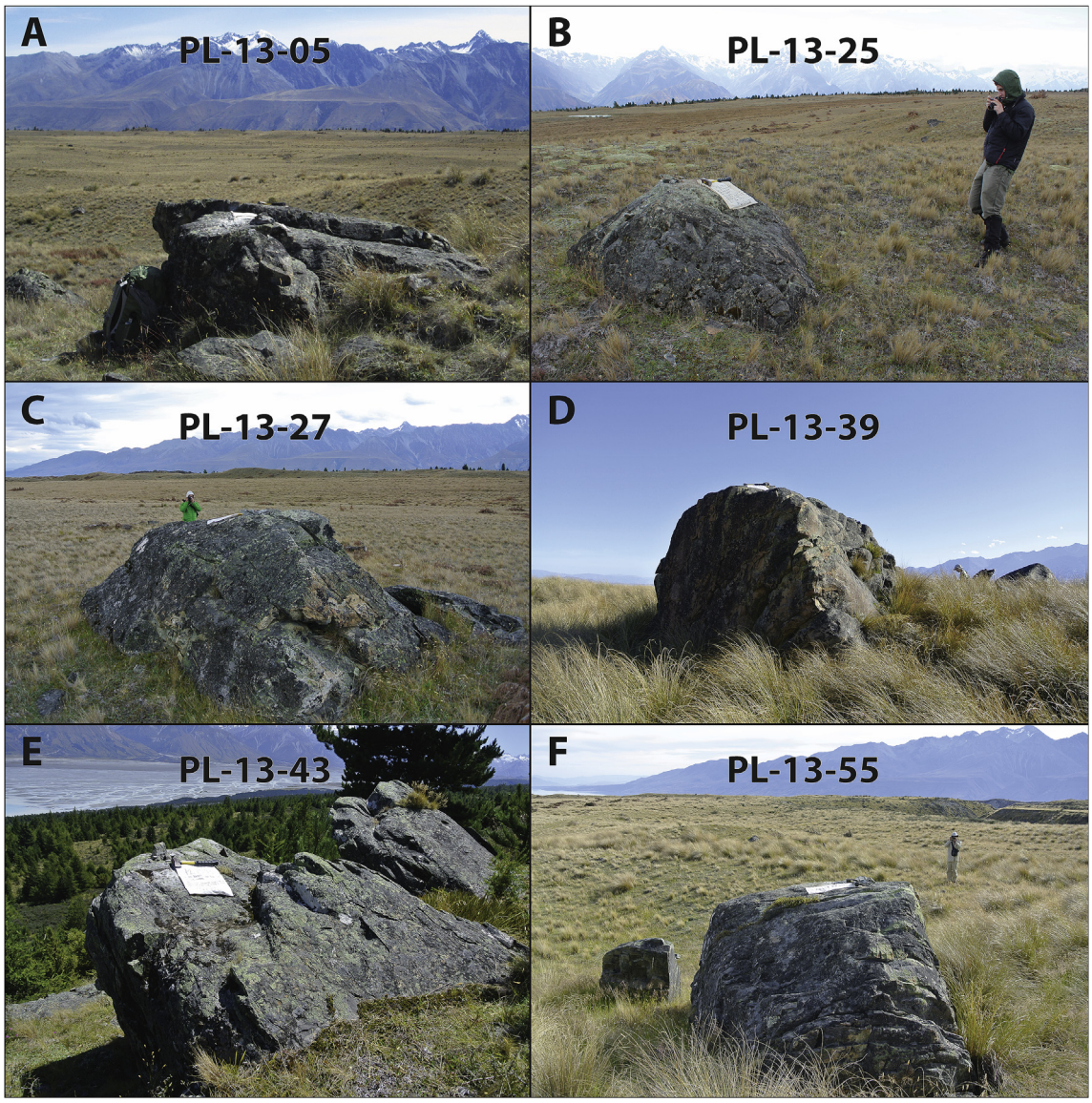

Fig. 5. Examples of boulders sampled for ^{10}Be surface-exposure dating. **A**. Westward view of a c. 1 m high boulder on moraine belt 5 from which sample PL-13-05 was collected. **B**. We obtained sample PL-13-25 from this c. 0.7 m high boulder in a broad ridge crest of moraine belt 4, seen looking northwest. **C**. This large boulder protruding from a subdued ridge of moraine belt 3 yielded sample PL-13-27; prominent ridges of moraine belt 2 are evident in the mid-ground of this southwesterly vantage. **D**. Southward view of the ~2.4 m high boulder in a ridge of moraine belt 2 from which sample PL-13-39 came. **E**. View northwest of the collection site of sample PL-13-43 on a large boulder embedded at the crest of the evacuated ice-contact slope of moraine belt 1. **F**. Sample PL-13-55 was taken from this boulder in moraine belt 3, viewed towards the southwest.

46,680 ± 760 yrs. The two youngest ages, 34,050 ± 670 yrs and 39,140 ± 770 yrs of samples PL-13-01 and PL-13-04, are more than two standard deviations younger than the arithmetic mean of the landform derived from all the ages. Moreover, these two ages are out of morphostratigraphic order in that they are younger than the mean age of moraine belt 5 (see below). For these reasons we consider these ages to be outliers and accordingly exclude them from further discussion. The remaining eight ages give an arithmetic mean ± SEM and production rate uncertainty age for moraine belt 6 of 44,000 ± 1000 yrs.

5.2. Moraine belt 5

Five ages from moraine belt 5 range from 39,460 ± 740 yrs to 43,860 ± 830 yrs. Moraine belt 5 is separated from Moraine belt 6 by a narrow outwash channel, demonstrating that it represents a distinct glacier fluctuation event. All samples are in morphostratigraphic order, and thus none is considered an outlier. The five ages afford a moraine belt 5 mean age of 41,800 ± 1100 yrs.

5.3. Moraine belt 4

Six ages from moraine belt 4 range from 35,340 ± 580 yrs to 40,540 ± 640 yrs. The oldest age of 40,540 ± 640 yrs (sample PL-13-18), is more than two standard deviations older than the arithmetic mean of all the other ages from moraine belt 4, and therefore is considered an outlier on that basis. The mean of the remaining five ages for moraine belt 4 is 36,450 ± 940 yrs.

5.4. Moraine belt 3

We processed six samples from moraine belt 3. Four of the ages show very good consistency and give a mean age of 26,730 ± 740 yrs. Samples PL-13-29 and PL-13-26 afford ages of

Table 1
^{10}Be data.

Sample ID	CAMS Laboratory number	Latitude (DD)	Longitude (DD)	Elevation (m.a.s.l.)	Boulder Size (L x W x H) (cm)	Sample Thickness (cm)	Density (g cm^{-2})	Shielding correction	Quartz weight (g)	Carrier added (g)	Carrier conc. (ppm)	^{10}Be/^{9}Be ± 1σ (10^{-14})	[^{10}Be] ± 1σ (10^{4}) (atoms/gram)	AMS std
Pukaki Left Lateral Ridge 6														
PL-13-01	BE35538	−43.8762010	170.2334727	1053.30	190 × 90 x 35	2.218	2.7	0.9996	4.0125	0.1800	1030	10.61 ± 0.21	32.58 ± 0.63	07KNSTD
PL-13-02	BE35539	−43.8768281	170.2331021	1052.96	340 × 270 x 163	3.657	2.7	0.9984	4.3002	0.1797	1030	14.54 ± 0.21	41.66 ± 0.62	07KNSTD
PL-13-03	BE35540	−43.8770557	170.2330881	1053.22	230 × 130 x 59	2.361	2.7	0.9978	2.9600	0.1805	1030	10.08 ± 0.15	42.09 ± 0.62	07KNSTD
PL-13-04	BE35541	−43.8782535	170.2335723	1049.54	250 × 230 x 80	1.660	2.7	0.9994	3.3653	0.1810	1030	10.19 ± 0.20	37.53 ± 0.73	07KNSTD
PL-13-05	BE35542	−43.8782604	170.2335552	1049.05	370 × 230 x 98	2.094	2.7	0.9974	5.0257	0.1781	1030	16.87 ± 0.33	41.01 ± 0.80	07KNSTD
PL-13-06	BE35543	−43.8790946	170.2339441	1051.74	360 × 140 x 80	1.686	2.7	0.9995	5.0339	0.1808	1030	17.71 ± 0.34	43.64 ± 0.84	07KNSTD
PL-13-07	BE35544	−43.8795281	170.2340870	1053.28	480 × 190 x 213	1.671	2.7	0.9977	5.1007	0.1815	1030	16.53 ± 0.32	40.36 ± 0.78	07KNSTD
PL-13-08	BE35546	−43.8796105	170.2339787	1051.28	300 × 110 x 120	1.149	2.7	0.9992	5.0523	0.1805	1030	17.44 ± 0.33	42.66 ± 0.80	07KNSTD
PL-13-09	BE35547	−43.8796407	170.2339218	1053.08	210 × 150 x 160	1.370	2.7	0.9995	5.0861	0.1815	1030	18.43 ± 0.30	45.04 ± 0.73	07KNSTD
PL-13-13	BE35550	−43.8729321	170.2337422	1061.15	170 × 140 x 78	1.180	2.7	0.9794	5.0075	0.1823	1030	16.62 ± 0.31	41.43 ± 0.77	07KNSTD
Pukaki Left Lateral Ridge 5														
PL-13-10	BE35548	−43.8772249	170.2323728	1046.61	260 × 160 x 58	1.290	2.7	0.9991	5.1179	0.1820	1030	15.55 ± 0.29	37.84 ± 0.71	07KNSTD
PL-13-11	BE35549	−43.8773703	170.2319382	1042.69	370 × 120 x 80	1.570	2.7	0.9975	5.0450	0.1816	1030	16.15 ± 0.33	39.79 ± 0.81	07KNSTD
PL-13-14	BE35551	−43.8782505	170.2306563	1039.41	320 × 160 x 53	1.490	2.7	0.9993	5.1853	0.1820	1030	16.62 ± 0.33	39.93 ± 0.78	07KNSTD
PL-13-15	BE35552	−43.8778197	170.2318044	1041.11	130 × 90 x 50	1.240	2.7	0.9925	5.1433	0.1817	1030	17.25 ± 0.32	41.74 ± 0.78	07KNSTD
PL-13-20	BE35558	−43.8708948	170.2309583	1063.65	170 × 140 x 48	2.320	2.7	0.9963	5.0800	0.1816	1030	16.48 ± 0.26	40.51 ± 0.64	07KNSTD
Pukaki Left Lateral Ridge 4														
PL-13-16	BE35554	−43.8739854	170.2299800	1049.47	120 × 90 x 50	2.165	2.7	0.9988	5.0196	0.1823	1030	14.69 ± 0.24	36.69 ± 0.61	07KNSTD
PL-13-17	BE35555	−43.8744294	170.2301698	1048.31	150 × 100 x 50	2.959	2.7	0.9996	5.0240	0.1829	1030	13.46 ± 0.23	33.70 ± 0.58	07KNSTD
PL-13-18	BE35556	−43.8746523	170.2300894	1047.48	230 × 170 x 80	2.636	2.7	0.9993	5.2100	0.1815	1030	16.10 ± 0.25	38.56 ± 0.60	07KNSTD
PL-13-19	BE35557	−43.8747295	170.2304122	1051.18	230 × 190 x 88	1.831	2.7	0.9996	5.0753	0.1809	1030	13.98 ± 0.21	34.26 ± 0.52	07KNSTD
PL-13-23	BE35559	−43.8827683	170.2288606	1023.46	180 × 160 x 50	1.623	2.7	0.9997	5.1157	0.1824	1030	13.56 ± 0.19	33.24 ± 0.47	07KNSTD
PL-13-24	BE35560	−43.8830783	170.2292259	1023.55	550 × 260 x 118	1.504	2.7	0.9997	5.0626	0.1808	1030	14.20 ± 0.23	34.88 ± 0.58	07KNSTD
Pukaki Left Lateral Ridge 3														
PL-13-25	BE35733	−43.8902720	170.2260151	1006.10	180 × 150 x 68	1.380	2.7	0.9997	5.0915	0.1812	1030	9.65 ± 0.20	23.58 ± 0.48	07KNSTD
PL-13-26	BE35734	−43.8903248	170.2257816	1005.02	180 × 130 x 83	1.000	2.7	0.9997	5.2136	0.1816	1030	12.11 ± 0.22	28.97 ± 0.53	07KNSTD
PL-13-27	BE35735	−43.8905022	170.2250619	998.06	370 × 280 x 125	1.597	2.7	0.9997	5.1506	0.1818	1030	10.11 ± 0.21	24.48 ± 0.50	07KNSTD
PL-13-28	BE35736	−43.8708266	170.2257898	1060.83	170 × 120 x 40	1.495	2.7	0.9997	5.2007	0.1807	1030	11.32 ± 0.22	27.00 ± 0.53	07KNSTD
PL-13-29	BE35737	−43.8767101	170.2271148	1048.02	150 × 110 x 83	2.299	2.7	0.9997	5.2060	0.1808	1030	8.84 ± 0.23	21.05 ± 0.54	07KNSTD
PL-13-55	BE35738	−43.9068664	170.2312122	962.84	510 × 210 x 165	2.409	2.7	0.9998	5.1577	0.1811	1030	10.05 ± 0.18	24.21 ± 0.43	07KNSTD
Pukaki Left Lateral Ridge 2														
PL-13-31	BE35728	−43.8954737	170.2218269	983.61	650 × 480 x 145	1.833	2.7	0.9998	6.2033	0.1794	1030	8.84 ± 0.18	17.57 ± 0.37	07KNSTD
PL-13-32	BE35729	−43.8962120	170.2219523	980.96	370 × 290 x 210	2.297	2.7	0.9998	6.1859	0.1816	1030	8.66 ± 0.18	17.47 ± 0.36	07KNSTD
PL-13-33	BE35730	−43.8975257	170.2236001	979.24	520 × 280 x 143	1.342	2.7	0.9998	6.1460	0.1814	1030	8.97 ± 0.18	18.19 ± 0.38	07KNSTD
PL-13-34	BE35740	−43.9008178	170.2187226	962.46	440 × 360 x 248	1.133	2.7	0.9998	6.0943	0.1794	1030	8.50 ± 0.16	17.14 ± 0.33	07KNSTD
PL-13-36	BE35741	−43.8830397	170.2145901	1002.51	440 × 200 x 203	2.705	2.7	0.9997	6.1175	0.1816	1030	9.20 ± 0.18	18.72 ± 0.37	07KNSTD
PL-13-37	BE35742	−43.8748334	170.2158747	1030.87	380 × 240 x 138	2.041	2.7	0.9997	6.1135	0.1814	1030	9.11 ± 0.21	18.53 ± 0.44	07KNSTD
PL-13-38	BE35743	−43.8682733	170.2191957	1047.22	180 × 160 x 153	2.254	2.7	0.9996	5.5104	0.1816	1030	8.89 ± 0.17	20.09 ± 0.39	07KNSTD
PL-13-39	BE35731	−43.8703109	170.2214494	1053.26	520 × 300 x 238	1.498	2.7	0.9997	6.2005	0.1816	1030	9.65 ± 0.19	19.42 ± 0.38	07KNSTD
Pukaki Left Lateral Ridge 1														
PL-13-40	BE35745	−43.8933909	170.2106441	960.43	480 × 340 x 180	1.112	2.7	0.9998	5.9662	0.1812	1030	7.90 ± 0.16	16.44 ± 0.33	07KNSTD
PL-13-46	BE35746	−43.9194432	170.2229888	908.79	210 × 130 x 63	2.759	2.7	0.9999	7.2235	0.1816	1030	8.91 ± 0.25	15.35 ± 0.43	07KNSTD
PL-13-47	BE35747	−43.9284710	170.2264772	897.14	480 × 280 x 263	1.570	2.7	0.9999	5.9669	0.1818	1030	7.28 ± 0.15	15.18 ± 0.32	07KNSTD
PL-13-56	BE35748	−43.9308899	170.2218229	851.48	1650 × 660 x 423	2.740	2.7	0.9996	7.1269	0.1807	1030	8.13 ± 0.15	14.12 ± 0.27	07KNSTD
PL-13-58	BE35749	−43.9290741	170.2225842	870.80	500 × 310 x 225	2.600	2.7	0.9990	7.0434	0.1811	1030	8.17 ± 0.16	14.39 ± 0.29	07KNSTD

Table 2
^{10}Be surface-exposure ages (in thousands of cal. yrs before AD 2013; ± 1σ) from the Pukaki moraines. Outlying ages are italicized and marked by an asterisk (*) next to the sample ID. Bold ages ('Lm') are those discussed in text.

Sample ID	St age (ka)	Lm age (ka)
Pukaki Left Lateral Ridge 6		
*PL-13-01**	*34.79 ± 0.68*	***34.05 ± 0.67***
PL-13-02	45.15 ± 0.67	**43.90 ± 0.66**
PL-13-03	45.19 ± 0.68	**43.95 ± 0.66**
*PL-13-04**	*40.08 ± 0.79*	***39.14 ± 0.77***
PL-13-05	44.09 ± 0.87	**42.89 ± 0.85**
PL-13-06	46.61 ± 0.91	**45.32 ± 0.89**
PL-13-07	43.09 ± 0.84	**41.94 ± 0.82**
PL-13-08	45.40 ± 0.86	**44.15 ± 0.83**
PL-13-09	47.96 ± 0.79	**46.68 ± 0.76**
PL-13-13	44.61 ± 0.84	**43.38 ± 0.82**
Pukaki Left Lateral Ridge 5		
PL-13-10	40.41 ± 0.76	**39.46 ± 0.74**
PL-13-11	42.81 ± 0.88	**41.69 ± 0.86**
PL-13-14	42.98 ± 0.85	**41.85 ± 0.83**
PL-13-15	45.10 ± 0.85	**43.86 ± 0.83**
PL-13-20	43.18 ± 0.69	**42.02 ± 0.67**
Pukaki Left Lateral Ridge 4		
PL-13-16	39.36 ± 0.66	**38.45 ± 0.64**
PL-13-17	36.34 ± 0.64	**35.54 ± 0.62**
*PL-13-18**	*41.58 ± 0.66*	***40.54 ± 0.64***
PL-13-19	36.55 ± 0.56	**35.74 ± 0.55**
PL-13-23	36.19 ± 0.51	**35.41 ± 0.50**
PL-13-24	37.95 ± 0.63	**37.12 ± 0.62**
Pukaki Left Lateral Ridge 3		
PL-13-25	25.90 ± 0.53	**25.39 ± 0.52**
*PL-13-26**	*31.81 ± 0.59*	***31.06 ± 0.57***
PL-13-27	27.12 ± 0.56	**26.55 ± 0.55**
PL-13-28	28.46 ± 0.57	**27.82 ± 0.55**
*PL-13-29**	*22.52 ± 0.58*	***22.16 ± 0.57***
PL-13-55	27.74 ± 0.49	**27.17 ± 0.48**
Pukaki Left Lateral Ridge 2		
PL-13-31	19.68 ± 0.42	**19.49 ± 0.41**
PL-13-32	19.68 ± 0.41	**19.48 ± 0.41**
PL-13-33	20.38 ± 0.43	**20.16 ± 0.42**
PL-13-34	19.43 ± 0.38	**19.25 ± 0.37**
PL-13-36	20.81 ± 0.41	**20.56 ± 0.40**
PL-13-37	20.03 ± 0.48	**19.81 ± 0.47**
PL-13-38	21.49 ± 0.42	**21.19 ± 0.41**
PL-13-39	20.55 ± 0.40	**20.30 ± 0.40**
Pukaki Left Lateral Ridge 1		
PL-13-40	18.66 ± 0.38	**18.51 ± 0.37**
PL-13-46	18.37 ± 0.52	**18.24 ± 0.52**
PL-13-47	18.17 ± 0.38	**18.05 ± 0.38**
PL-13-56	17.68 ± 0.34	**17.58 ± 0.34**
PL-13-58	17.74 ± 0.36	**17.64 ± 0.36**

22,160 ± 570 yrs and 31,060 ± 570 yrs, respectively, and are not in morphostratigraphic order with respect to adjacent moraine belts. Thus we consider these ages to be outliers and do not include them in assessing the overall age of the moraine belt.

5.5. Moraine belt 2

Moraine belt 2 is 0.5 km wide and has clear continuity throughout the study area (Fig. 7). Eight samples were collected, from positions throughout the moraine belt, including its inboard and outboard margins. All ages overlap within error and no outliers are identified. The mean of all eight ages for moraine belt 2 is 20,030 ± 460 yrs.

5.6. Moraine belt 1

Five ages from moraine belt 1 are tightly clustered with good internal consistency and give a mean age of 18,000 ± 400 yrs. The three oldest ages are from the outer margin of the moraine belt (labelled 1 or 1b in Fig. 7), while the two youngest ages are from samples located on ice-recessional topography, ridge 1a, located 350 m inboard of and 100 m below the outer edge of the moraine belt (Fig. 5). The ages of three outer afford a landform age of 18,260 ± 390 yrs, while the two inner samples afford a landform age of 17,610 ± 350 yrs. Despite temptation to correlate these two sectors of the Pukaki moraine belt with similar-age components with the Ohau moraine sequence, the small number of samples, whose ages all overlap within error, calls for a conservative approach whereby all five ages from moraine belt 1 are combined in our statistical analysis and discussion.

6. Discussion

The chronology of moraine belts preserved along the left-lateral margin of the Pukaki glacier trough demonstrates that the Southern Alps climate record features a millennial-scale pulsebeat of glacier extent during MIS 4, 3, and 2 (Kelley et al., 2014; Doughty et al., 2015; Schaefer et al., 2015). Glacial geomorphologic mapping and surface-exposure age dating shows that episodes of Pukaki glacier recession had striking similarity in timing to millennial-scale climate changes recognized in the paleoclimate record. Glacier recession occurred during Heinrich stadials and glacier expansion occurred between the stadials. The correspondence between Heinrich stadials and Southern Alps glaciers is particularly evident during the last glacial termination, when two episodes of recession, which together transitioned the Pukaki glacier from a full-glacial to a Holocene configuration, coincided, respectively, with Heinrich stadial 1 (HS 1) and Heinrich stadial 0 (HS 0 or Younger Dryas) (Putnam et al., 2010a, 2013a; 2013b; Kaplan et al., 2010, 2013; Kelley et al., 2014; Doughty et al., 2015). This apparent anti-phased coupling between the hemispheres on a millennial timescale possibly reflects the operation of a north-south temperature seesaw, either through the ocean or

Table 3
Summary statistics for Pukaki moraine ^{10}Be surface-exposure age distributions. Bold ages are those discussed in the text.

Data set	*n*	*n* out	Mean Age (yrs)	± SEM Unc (yrs)	±1σ (yrs)	± SEM + P-rate Uncertainty (yrs)	Error-weighed mean (yrs)	Error weighted uncertainty (yrs)	Peak age (yrs)	Median age (yrs)	χ^2	Reduced χ^2
Moraine belt 6 (all)	10	–	42,500	1100	3600	1400	42,270	240	43,820	43,640	235.86	26.21
Moraine belt 6 (outliers excluded)	8	2	**44,000**	510	1500	**1000**	44,000	270	43,820	43,930	23.18	3.31
Moraine belt 5 (all)	5	–	**41,800**	700	1600	**1100**	41,700	350	41,920	41,850	16.22	4.05
Moraine belt 4 (all)	6	–	37,100	830	2000	1100	36,900	240	35,560	36,430	57.51	11.50
Moraine belt 4 (outliers excluded)	5	1	**36,450**	590	1300	**940**	36,300	260	35,570	35,740	19.03	4.76
Moraine belt 3 (all)	6	–	26,700	1200	2900	1300	26,690	220	27,150	26,860	132.87	26.57
Moraine belt 3 (outliers excluded)	4	2	**26,730**	520	1000	**740**	26,730	260	27,150	26,860	11.37	3.79
Moraine belt 2 (all)	8	–	**20,030**	230	650	**460**	20,020	140	19,640	19,980	18.32	2.62
Moraine belt 1 (all)	5	–	**18,000**	180	390	**400**	17,950	170	17,810	18,050	4.63	1.16
Moraine belt 1a	2	–	**17,610**	30	40	**350**	17,610	240	17,610	17,610	0.01	0.01
Moraine belt 1b	3	–	**18,260**	130	230	**390**	18,270	240	18,280	18,240	0.34	0.37

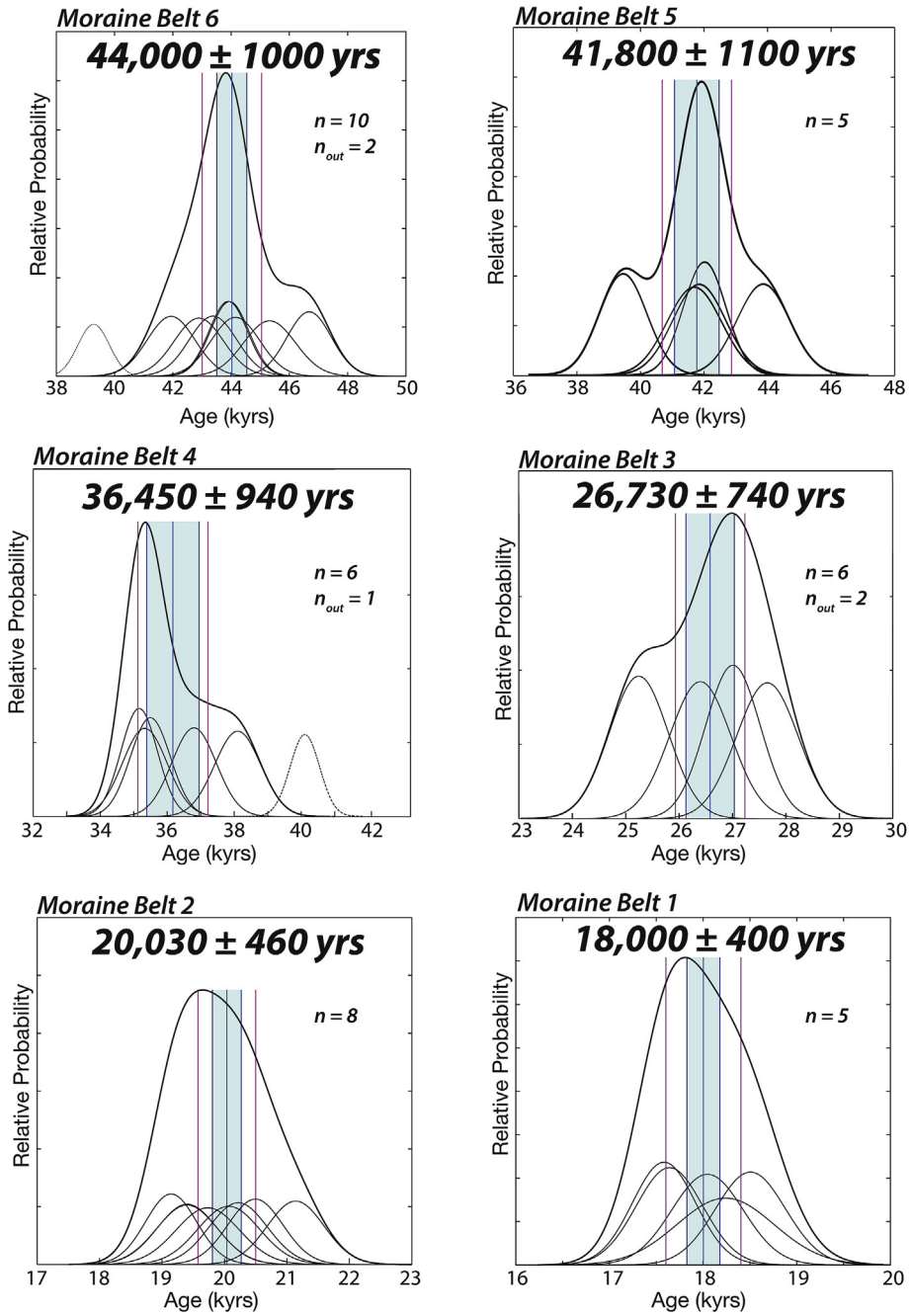

Fig. 6. Probability density functions (i.e.,'camelplots') for the six Pukaki moraine belts in the field area. Center blue line is arithmetic mean, while vertical black and purple lines are standard error of the mean (SEM) and production rate uncertainty thresholds, respectively. The thin black curves are the Gaussian representation of each sample. Dotted black lines represent outliers. The thick black curve is the total probability distribution of all plotted samples, excluding outliers. The associated statistics are presented in Table 3.

atmosphere, in which winter-centric Heinrich stadials correspond with southern shifts of the earth's thermal equator, the Southern Hemisphere westerly wind belt, the Australasian monsoon system, and the Subtropical Front (STF) at the outer edge of the Southern Ocean (Denton et al., 2010). Our results show that distinct pulses of glaciation in the Southern Alps can be sufficiently differentiated using thorough geomorphologic mapping together with surface-exposure age dating.

6.1. Moraine chronology

The ^{10}Be chronology of the left-lateral moraine belts indicates that the Pukaki glacier achieved multiple maxima during MIS 3 and 2. The oldest dated moraine indicates that the maximum yet-recognized MIS 3 extent of the Pukaki glacier was achieved 44,000 ± 1000 yrs ago. Ages of inboard moraine belts of 41,800 ± 1100 yrs; 36,450 ± 940 yrs; 26,730 ± 740 yrs; and 20,030 ± 460 yrs demonstrate that the left-lateral margin of the Pukaki glacier reached close to its maximum areal extent several times during, and prior to, the classic global LGM. The moraine belt with an age of 18,000 ± 400 yrs represents the final maximal extent of the Pukaki glacier within the LLGM moraine belts, at the onset of post-glacial retreat.

The ^{10}Be chronology given here for the northern sector of the

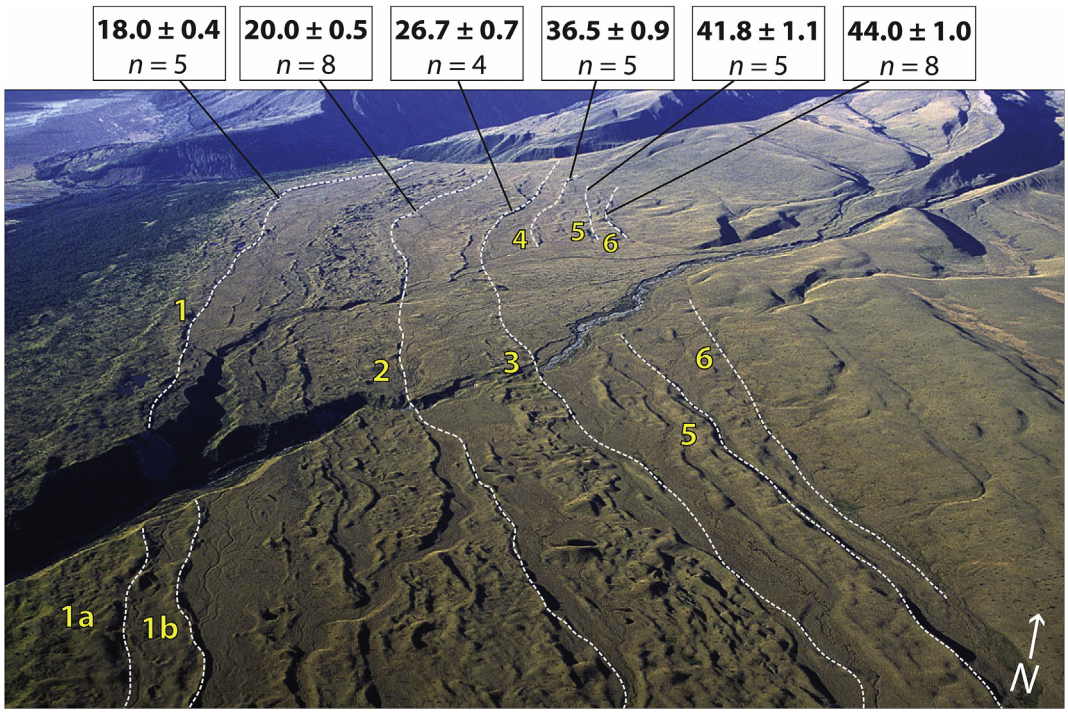

Fig. 7. Oblique aerial view north-northwest across the study area. White dotted line indicates the outer limit of each moraine belt, with belt numbering in yellow and mean age of each belt annotated at top. The vantage position is indicated in Fig. 2. Photo: G.H. Denton.

upper-left-lateral moraines of the Pukaki glacier is consistent with other published ^{10}Be chronologies from correlative moraine belts dated on adjacent parts of the Pukaki left-lateral moraine system. Moraine belt 5, deposited 41,800 ± 1100 yrs ago, is correlated with a same-age moraine of Kelley et al. (2014). Moraine belts formed along the upper reaches of the Pukaki left-lateral at 36,450 ± 940 yrs ago, 26,730 ± 740 yrs ago, and 20,030 ± 460 yrs ago confirm the findings of moraines formed at 36,800 ± 1600 yrs ago, 27,100 ± 100 yrs ago, 20,270 ± 770 yrs ago, and 18,130 ± 440 yrs ago elsewhere around Lake Pukaki (Doughty et al., 2015; Kelley et al., 2014) (Fig. 8). The late-glacial Birch Hill moraines deposited by the former Pukaki glacier were formed 14,090 ± 300 yrs ago (n = 2) and 12,970 ± 360 yrs ago (n = 21) (Putnam et al., 2010a).

6.2. Heinrich pulsebeat

A primary objective of our study was to test the relationship between Southern Hemisphere mid-latitude glacial maxima and millennial-scale global climate events. The chronology presented here indicates anti-phased timing of maximum glacial extents and Heinrich stadials. Glacier expansion occurred between Heinrich stadials, with glacier retreat occurring during Heinrich stadials (Fig. 8). A particularly intriguing finding is the ages of moraine belts 6 and 5. These belts are geomorphically distinct, separated by an outwash channel, and therefore represent separate moraine-forming events, about 2000 years apart based on the mean moraine ages. This opens up the possibility that they mark an inter-Heinrich stadial glacial fluctuation, and we speculate that these two moraine belts may relate to Dansgaard–Oeschger (D-O) oscillation #11 (Barker and Diz, 2014). We note that the dating uncertainties preclude a firm interpretation in absence of further investigation. Nevertheless, these findings hint at a potential teleconnection between the climate of New Zealand and the North Atlantic region on a millennial-scale.

Moraine belts representing the extent of the Ohau glacier during the LLGM (Fig. 2) have ages of 32,520 ± 970 yrs (n = 6), 22,510 ± 660 yrs (n = 24), 18,220 ± 500 yrs (n = 18), and 17,690 ± 350 yrs (n = 6) (Putnam et al., 2013a). Differences in the age structure of the Ohau and Pukaki moraine belt sequences are unlikely to reflect climatic contrasts because they occupy adjacent catchments of broadly similar character and climatic regime. The age differences more likely indicate chance vagaries in moraine preservation, arising from minor differences of morphometry and altitudinal geometry in each catchment, its trunk valley and proximal foreland. It has been estimated that in any given glacier system, roughly only three per every ten glacier advances will leave moraines that survive in the long term, as a result of small geometric differences, despite similar snowline changes (Gibbons et al., 1984). The youngest LLGM moraines of the Ohau glacier and Pukaki glacier are coeval because there was no subsequent glacier advance to overprint or alter them. Following the approach of Doughty et al. (2015), a diagram comparing the LLGM moraine chronologies of the Pukaki glacier and the Ohau glacier is presented in Fig. 8. This highlights a composite record of episodes of lateral or terminal moraine formation. Expressed as mean ages of moraine belts in kyrs and neglecting uncertainty ranges, these episodes occurred at c. 65 kyrs ago, c. 44 kyrs ago, c. 42 kyrs ago, c. 36 kyrs ago, c. 32.5 kyrs ago, c. 27 kyrs ago, c. 22.5 kyrs ago, c. 21-20 kyrs ago and c. 18 kyrs ago. These results highlight more complexity in Last Glaciation climate variations than shown in the Southern Alps composite glacier advance record presented by Shulmeister et al. (2019). For example, that compilation does not recognize an ice advance around c. 44-42 kyrs ago, but our morphological record coupled with dating illustrates at least two separate moraine-forming events at about that time.

The millennial-scale pulsebeat pattern of glacier extent resembling Heinrich stadials is not unique to glacier systems of central South Island, New Zealand, but rather appears to be at least pan-Pacific in the middle latitudes of the Southern Hemisphere. In the

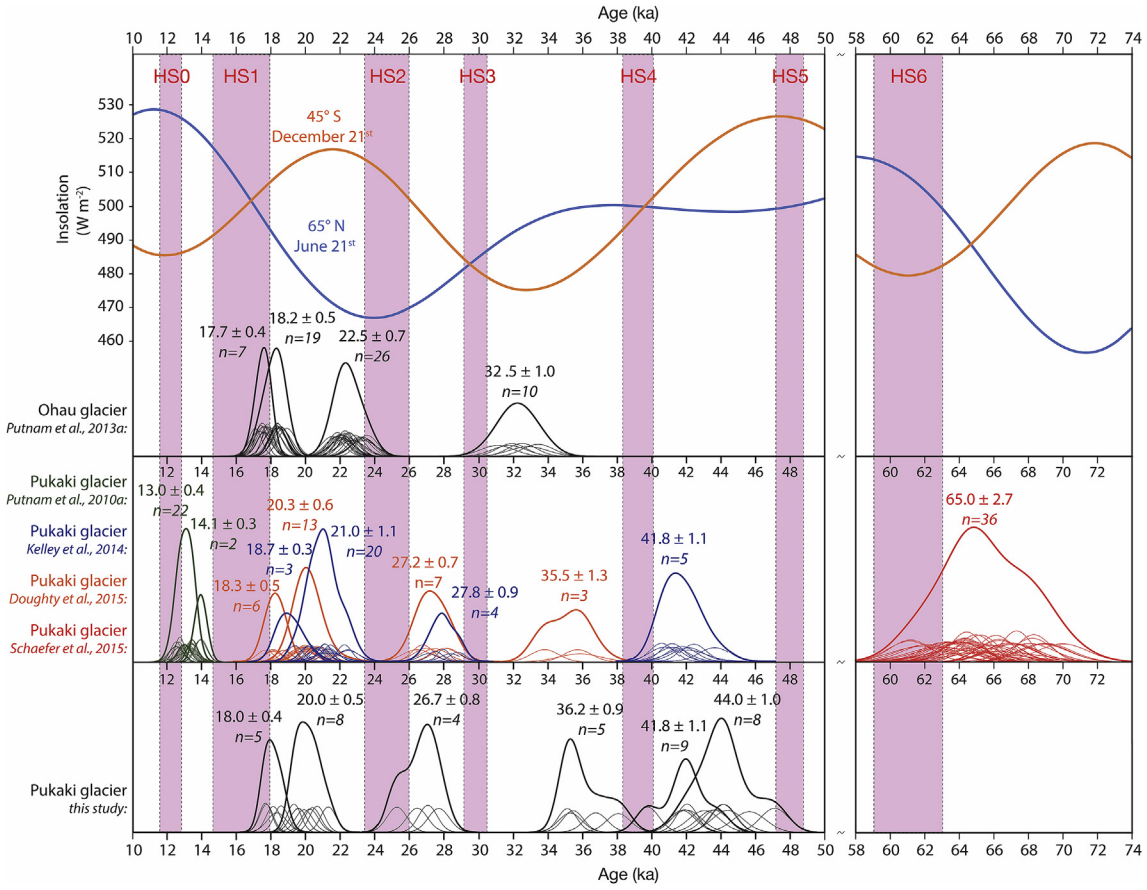

Fig. 8. Heinrich pulsebeat of New Zealand Southern Alps glaciers from ~10 to 50 kyrs. Pukaki glacier moraine chronologies from this study are compared with those of Kelley et al. (2014) and Doughty et al. (2015). Ohau glacier chronology is from Putnam et al. (2013a). Red bands correspond to Heinrich stadials. The timing of Heinrich stadials is defined by isotopic excursions in Chinese speleothems (Cheng et al., 2009; Wang et al., 2001, 2008).

Chilean Lake District (39°- 43°S), ^{14}C ages document times when Andean glaciers overran terrestrial vegetation within the LGM moraine belt (Denton et al., 1999). Note that all ages given here for the Chilean Lake District are from ^{14}C dates (Denton et al., 1999; Moreno et al., 2015) that have been converted to calendar ages using the IntCal13 calibration (Reimer et al., 2013), as reported in Moreno et al. (2015). Formation of Pukaki left-lateral moraine belts correspond to glacier advances into the Llanquihue moraine belt in the Chilean Lake District, as documented by Denton et al. (1999). Formation of Pukaki moraine belt 3 (26,730 ± 740 yrs ago) was coeval with glacier advances recorded by till-buried soils at Seno Reloncavi (26,900 ± 190 yrs ago; n = 4; no outliers excluded), Puerto Montt (26,000 ± 70 yrs ago; n = 4; no outliers excluded) and Teguaco (26,790 ± 790 yrs ago; n = 12; 3 outliers excluded). Pukaki moraine belt 1 (age of 18,000 ± 400 yrs) correlates with Chilean Lake District glacier advances at Punta Penas (18,090 ± 90 yrs ago; n = 4; no outliers excluded) and Dalcahue (17,980 ± 70 yrs ago; n = 35; 5 outliers excluded).

6.3. Milankovitch hypothesis

To assess whether the Milankovitch (1941) hypothesis that summer insolation intensity drives glacier volume and extent is valid for the Southern Alps, we compared surface-exposure ages of the moraine belts against local summertime insolation intensity for 45°S latitude. A recent review notes that some Last Glaciation glacier advances were associated with local insolation minima (Otira 1, c. 65,000 yrs and Otira 4, c. 31,500 years) but other are attributed to changes in atmospheric circulation (Shulmeister et al., 2019). We find no correlation between the former Pukaki and Ohau glacier maxima and local summer insolation intensity, because moraine formation occurred during times of minimum, maximum, and intermediate insolation intensity values at 45°S (Fig. 8). Furthermore, Pukaki or Ohau glacier fluctuation did not follow Northern Hemisphere summer insolation intensity at 65°N, nor insolation signals at any latitude. We therefore conclude that variations in summertime insolation intensity were not responsible for driving the areal extent of the Pukaki glacier through direct radiative forcing nor climate teleconnections.

6.4. Heinrich stadial 1 deglaciation

The rapid retreat of the Pukaki glacier from moraine belt 1 corresponds with the onset of HS 1 (as defined by Barker et al., 2009). Thus, the beginning of HS 1 was coincident with the largest preserved ice retreat of the Pukaki glacier and brought the LLGM to a rapid close in New Zealand (Denton et al., 2010). Reconstructing the magnitude of each previous recession of the Pukaki glacier during LLGM glacier fluctuations is not possible due to destruction and/or burial of evidence by younger advances and their resultant moraine sequences. However, the Pukaki moraine belt 1 represents the last major stand of the LLGM glacier, and records the subsequent onset of retreat. The steep, hummocky, and chaotic nature of landforms in moraine belt 1 suggests that retreat was rapid. The age of the outboard part of moraine belt 1, 18,000 ± 400 yrs, indicates that the onset of glacial retreat was coeval with the onset of HS 1, and Barrell and Read (2014) show that at least c. 400 m of downwasting and c. 30 km of terminal retreat of

the Pukaki glacier had occurred prior to 16,170 ± 890 cal yrs ago (i.e. during HS 1). Putnam et al. (2010a) argue on morphological grounds that post-LLGM recession saw the Pukaki glacier withdraw up-valley of the position subsequently attained by the Birch Hill ice advance, representing at least c. 35 km of terminal retreat after c. 18,000 yrs ago. However, evidence for the minimum ice position following the LLGM was erased by the Birch Hill advance during the Antarctic Cold Reversal (Putnam et al., 2010a).

By 14,090 ± 300 yrs, and subsequently at 13,120 ± 300 yrs and 12,970 ± 300 yrs, the Pukaki glacier margins were located at or inboard of the moraine belt at Birch Hill (Putnam et al., 2010a). Retreat from the Birch Hill position around 13,000 yrs indicates that ice recession also occurred during HS 0 (i.e., the Younger Dryas stadial), as in the nearby Rakaia valley (Koffman et al., 2017) and Ohau valley (Kaplan et al., 2010), similar to previous Heinrich stadials.

7. Conclusions

1. A ^{10}Be surface-exposure chronology, comprising 41 new dates on left-lateral glacial landforms near Lake Pukaki, indicates that the Pukaki glacier achieved six distinct maxima at 44,000 ± 1000 yrs ago (n = 8); 41,800 ± 1100 yrs ago (n = 5); 36,450 ± 940 yrs ago (n = 5); 26,730 ± 740 yrs ago (n = 4); 20,030 ± 460 yrs ago (n = 8); and 18,000 ± 400 yrs ago (n = 5). This chronology confirms other research undertaken near Lake Pukaki by Schaefer et al. (2006, 2015); Putnam et al. (2010a), Kelley et al. (2014) and Doughty et al. (2015). These data indicate that the Pukaki glacier reached close to its maximum areal extent multiple times during, and prior to, the classic global LGM.
2. The Pukaki glacier in the Southern Alps of New Zealand reveals a millennial-scale pulsebeat of glacier extent. Our ^{10}Be surface-exposure chronology for the upper left-lateral moraine belts at Lake Pukaki reinforce previous chronologies from Lake Pukaki and other Southern Alps catchments and adds to the chronological foundation of Southern Alps glacial history. Taken together with results from the Chilean Lake District of southern South America, the central Southern Alps glacial chronology signals a millennial pulsebeat of Southern Hemisphere atmospheric temperatures and glacier extent that resembles Heinrich stadials.
3. The six identified maxima of the Pukaki glacier spanned an entire cycle of orbital variations in summer insolation intensity at the latitude of the Southern Alps (45°S). These data show that fluctuations in the size of the Pukaki glacier were not tied directly to local nor far-field summer insolation intensity values on orbital timescales.
4. This chronology provides further evidence for rapid glacial retreat during the last glacial termination, coeval with the onset of the HS 1. An inter-Heinrich stadial glacier readvanced occurred during the Antarctic Cold Reversal, followed by retreat during HS 0 (the Younger Dryas).

Acknowledgements

This work was supported by funding from the Comer Family Foundation, the Quesada Family Foundation, the National Oceanographic and Atmospheric Administration (NOAA), and the National Science Foundation (grant no. 1102782). Strand and Putnam acknowledge the National Science Foundation (grant no. 1554990) for support while writing this paper. D. Barrell was supported by GNS Science. We are grateful to K. Needleman for assistance with laboratory work, and to T. and K. Ritchie of Lake Ruataniwha Holiday Park for a home-away-from-home during New Zealand field seasons. We thank Braemar Station and Mount Cook Station for generously granting access to their land. This is LDEO contribution #8338.

Appendix A. Supplementary data

Supplementary data related to this article can be found at https://doi.org/10.1016/j.quascirev.2019.07.022.

References

Anderson, B.M., Mackintosh, A.N., 2006. Temperature change is the major driver of late-glacial and Holocene glacier fluctuations in New Zealand. Geology 34, 121.
Anderson, B.M., Mackintosh, A.N., Stumm, D., George, L., Kerr, T., Winter-Billington, A., Fitzsimons, S.J., 2010. Climate sensitivity of a high-precipitation glacier in New Zealand. J. Glaciol. 56, 114–128.
Balco, G., Stone, J.O., Lifton, N.A., Dunai, T.J., 2008. A complete and easily accessible means of calculating surface exposure ages or erosion rates from ^{10}Be and ^{26}Al measurements. Quat. Geochronol. 3, 174–195.
Barker, S., Diz, P., Vautravers, M.J., Pike, J., Knorr, G., Hall, I.R., Broecker, W.S., 2009. Interhemispheric Atlantic seesaw response during the last deglaciation. Nature 457, 1097–1102.
Barker, S., Diz, P., 2014. Timing of the descent into the last Ice Age determined by the bipolar seesaw. Paleoceanography 29, 489–507.
Barrell, D.J.A., Andersen, B.G., Denton, G.H., 2011. Glacial geomorphology of the central South Island, New Zealand. GNS Sci. Monogr. 27, 71. Lower Hutt, New Zealand. Map.
Barrell, D.J.A., 2014. The balmoral moraines near Lake Pukaki, southern Alps: a new reference area for the early Otira glaciation in New Zealand. N. Z. J. Geol. Geophys. 57, 442–452.
Barrell, D.J.A., Read, S.A., 2014. The deglaciation of Lake Pukaki, South Island, New Zealand—a review. N. Z. J. Geol. Geophys. 57, 86–101.
Carter, L., et al., 1998. Ocean circulation New Zealand. In: NIWA Chart Miscellaneous Series, vol. 76. NIWA, Wellington.
Cheng, H., Edwards, R.L., Broecker, W.S., Denton, G.H., Kong, X., Wang, Y.-J., Zhang, R., Wang, X., 2009. Ice age terminations. Science 326, 248–252.
Clark, P.U., Mix, A.C., 2002. Ice sheets and sea level of the last glacial maximum. Quat. Sci. Rev. 21, 1–7.
Clark, P.U., Dyke, A.S., Shakun, J.D., Carlson, A.E., Clark, J., Wohlfarth, B., Mitrovica, J.X., Hostetler, S.W., McCabe, A.M., 2009. The last glacial maximum. Science 325, 710–714.
Cox, S.C., Barrell, D.J.A., 2007. Geology of the Aoraki Area. Institute of Geological and Nuclear Sciences 1:250,000 Geological Map 15. GNS Science. Lower Hutt, New Zealand, p. 71, 1 sheet.
Croll, James, 1875. Climate and Time in Their Geological Relations. A Theory of Secular Changes of the Earth's Climate. Appleton, New York.
De Deckker, P., Moros, M., Perner, K., Jansen, E., 2012. Influence of the tropics and southern westerlies on glacial interhemispheric asymmetry. Nat. Geosci. 5, 266–269.
Denton, G.H., Anderson, R.F., Toggweiler, J.R., Edwards, R.L., Schaefer, J.M., Putnam, A.E., 2010. The last glacial termination. Science 328, 1652–1656.
Denton, G.H., Lowell, T.V., Heusser, C.J., Schlüchter, C., Andersen, B.G., Heusser, L.E., Moreno, P.I., Marchant, D.R., 1999. Geomorphology, stratigraphy, and radiocarbon chronology of Llanquihue drift in the area of the southern Lake District, Seno Reloncavi, and Isla Grande de Chiloe, Chile. Geogr. Ann. Ser. A Phys. Geogr. 81, 167–229.
Doughty, A.M., Schaefer, J.M., Andersen, B.G., Putnam, A.E., Kaplan, M.R., Barrell, D.J.A., Denton, G.H., Finkel, R.C., Schwartz, R., 2015. Mismatch of glacier extent and summer insolation in southern hemisphere mid- latitudes. Geology 43, 407–410.
Gibbons, A.B., Megeath, J.D., Pierce, K.L., 1984. Probability of moraine survival in a succession of glacial advances. Geology 12, 327–330.
Golledge, N.R., Mackintosh, A.N., Anderson, B.M., Buckley, K.M., Doughty, A.M., Barrell, D.J.A., Denton, G.H., Vandergoes, M.J., Andersen, B.G., Schaefer, J.M., 2012. Last glacial maximum climate in New Zealand inferred from a modelled southern Alps icefield. Quat. Sci. Rev. 46, 30–45.
Hays, J.D., Imbrie, J., Shackleton, N.J., 1976. Variations in the Earth's orbit: pacemaker of the ice ages. Science 194, 1121–1132.
Kaplan, M.R., Schaefer, J.M., Denton, G.H., Barrell, D.J.A., Chinn, T.J.H., Putnam, A.E., Andersen, B.G., Finkel, R.C., Schwartz, R., Doughty, A.M., 2010. glacier retreat in New Zealand during the younger Dryas stadial. Nature 467, 194–197.
Kaplan, M.R., Schaefer, J.M., Denton, G.H., Doughty, A.M., Barrell, D.J.A., Chinn, T.J.H., Putnam, A.E., Andersen, B.G., Mackintosh, A.N., Finkel, R.C., Schwartz, R., Anderson, B.M., 2013. The anatomy of long-term warming since 15 ka in New Zealand based on net glacier snowline rise. Geology 41, 887–890.
Kelley, S.E., Kaplan, M.R., Schaefer, J.M., Andersen, B.G., Barrell, D.J.A., Putnam, A.E., Denton, G.H., Schwartz, R., Finkel, R.C., Doughty, A.M., 2014. High-precision ^{10}Be chronology of moraines in the Southern Alps indicates synchronous cooling in Antarctica and New Zealand 42,000 years ago. Earth Planet. Sci. Lett. 405, 194–206.
Kelly, M.A., Lowell, T.V., Hall, B.L., Schaefer, J.M., Finkel, R.C., Goehring, B.M.,

Alley, R.B., Denton, G.H., 2008. A ^{10}Be chronology of lateglacial and Holocene mountain glaciation in the Scoresby Sund region, east Greenland: implications for seasonality during lateglacial time. Quat. Sci. Rev. 27, 2273–2282.
Koffman, T.N.B., Schaefer, J.M., Putnam, A.E., Denton, G.H., Barrell, D.J.A., Rowan, A.V., Finkel, R.C., Rood, D.H., Schwartz, R., Plummer, M.A., Brocklehurst, S.H., 2017. A beryllium-10 chronology of late-glacial moraines in the upper Rakaia valley, Southern Alps, New Zealand supports Southern-Hemisphere warming during the Younger Dryas. Quat. Sci. Rev. 170, 14–25.
Lifton, N., Smart, B., Shea, M., 2008. Scaling time-integrated in situ cosmogenic nuclide production rates using a continuous geomagnetic model. Earth Planet. Sci. Lett. 268, 190–201.
Mackintosh, A.N., Anderson, B.M., Pierrehumbert, R.T., 2017. Reconstructing climate from glaciers. Annu. Rev. Earth Planet Sci. 45, 649–680.
Mercer, J.H., 1984. Simultaneous climatic change in both hemispheres and similar bipolar interglacial warming: evidence and implications. Clim. Process. Clim. Sensit. Am. Geophys. Union Geophys. Monogr. 29, 307–313.
McGlone, M.S., Moar, N.T., 1998. Dryland Holocene vegetation history, central Otago and the Mackenzie basin, South Island, New Zealand. N. Z. J. Bot. 36, 91–111.
Milankovitch, M., 1941. Kanon der Erdbestrahlung und seine Andwendung auf das Eiszeiten-problem. Royal Serbian Academy, Belgrade.
Mix, A.C., Bard, E., Schneider, R., 2001. Environmental processes of the ice age: land, oceans, glaciers (EPILOG). Quat. Sci. Rev. 20, 627–657.
Moreno, P.I., Denton, G.H., Moreno, H., Lowell, T.V., Putnam, A.E., Kaplan, M.R., 2015. Radiocarbon chronology of the last glacial maximum and its termination in northwestern Patagonia. Quat. Sci. Rev. 122, 233–249.
Nishiizumi, K., Imamura, M., Caffee, M.W., Southon, J.R., Finkel, R.C., McAninch, J., 2007. Absolute calibration of ^{10}Be AMS standards. Nucl. Instrum. Methods Phys. Res. Sect. B Beam Interact. Mater. Atoms 258, 403–413.
Oerlemans, J., 1994. Quantifying global warming from the retreat of glaciers. Science 264, 243–245.
Porter, S.C., 1975. Equilibrium-line altitudes of late quaternary glaciers in the southern Alps, New Zealand. Quat. Res. 5, 27–47.
Putnam, A.E., Denton, G.H., Schaefer, J.M., Barrell, D.J.A., Andersen, B.G., Finkel, R.C., Schwartz, R., Doughty, A.M., Kaplan, M.R., Schlüchter, C., 2010a. glacier advance in southern middle-latitudes during the Antarctic Cold Reversal. Nat. Geosci. 3, 700–704.
Putnam, A.E., Schaefer, J.M., Barrell, D.J.A., Vandergoes, M.J., Denton, G.H., Kaplan, M.R., Finkel, R.C., Schwartz, R., Goehring, B.M., Kelley, S.E., 2010b. In situ cosmogenic ^{10}Be production-rate calibration from the Southern Alps, New Zealand. Quat. Geochronol. 5, 392–409.
Putnam, A.E., Schaefer, J.M., Denton, G.H., Barrell, D.J.A., Finkel, R.C., Andersen, B.G., Schwartz, R., Chinn, T.J.H., Doughty, A.M., 2012. Regional climate control of glaciers in New Zealand and Europe during the pre-industrial Holocene. Nat. Geosci. 5, 627–630.
Putnam, A.E., Schaefer, J.M., Denton, G.H., Barrell, D.J.A., Birkel, S.D., Andersen, B.G., Kaplan, M.R., Finkel, R.C., Schwartz, R., Doughty, A.M., 2013a. The last glacial maximum at 44S documented by a ^{10}Be moraine chronology at Lake Ohau, southern Alps of New Zealand. Quat. Sci. Rev. 62, 114–141.
Putnam, A.E., Schaefer, J.M., Denton, G.H., Barrell, D.J.A., Andersen, B.G., Koffman, T.N.B., Rowan, A.V., Finkel, R.C., Rood, D.H., Schwartz, R., Vandergoes, M.J., Plummer, M.A., Brocklehurst, S.H., Kelley, S.E., Ladig, K.L., 2013b. Warming and glacier recession in the Rakaia valley, southern Alps of New Zealand, during Heinrich stadial 1. Earth Planet. Sci. Lett. 382, 98–110.
Reimer, P.J., Bard, E., Bayliss, A., Beck, J.W., 2013. IntCal13 and Marine13 radiocarbon age calibration curves 0–50,000 years cal BP. Radiocabron 55, 1869–1887.
Schaefer, J.M., Denton, G.H., Barrell, D.J.A., Ivy Ochs, S., Kubik, P.W., Andersen, B.G., Phillips, F.M., Lowell, T.V., Schlüchter, C., 2006. Near-synchronous interhemispheric termination of the last glacial maximum in mid-latitudes. Science 312, 1510–1513.
Schaefer, J.M., Denton, G.H., Kaplan, M.R., Putnam, A.E., Finkel, R.C., Barrell, D.J.A., Andersen, B.G., Schwartz, R., Mackintosh, A.N., Chinn, T.J.H., Schluchter, C., 2009. High-frequency Holocene glacier fluctuations in New Zealand differ from the northern signature. Science 324, 622–625.
Schaefer, J.M., Putnam, A.E., Denton, G.H., Kaplan, M.R., Birkel, S., Doughty, A.M., Kelley, S., Barrell, D.J.A., Finkel, R.C., Winckler, G., Anderson, R.F., Ninneman, U.S., Barker, S., Schwartz, R., Andersen, B.G., Schluechter, C., 2015. The southern glacial maximum 65,000 years ago and its unfinished termination. Quat. Sci. Rev. 114, 52–60.
Shulmeister, J., Thackray, G.D., Rittenour, T.M., Hyatt, O.M., 2018. Multiple glacial advances in the Rangitata Valley, South Island, New Zealand, imply roles for Southern Hemisphere westerlies and summer insolation in MIS 3 glacial advances. Quat. Res. 1–19.
Shulmeister, J., Thackray, G.D., Rittenour, T.M., Fink, D., Patton, N.R., 2019. The timing and nature of the last glacial cycle in New Zealand. Quat. Sci. Rev. 206, 1–20.
Stone, J.O., 2000. Air pressure and cosmogenic isotope production. J. Geophys. Res. 105, 23753–23759.
Wang, Y.J., Cheng, H., Edwards, R.L., An, Z.S., Wu, J.Y., Shen, C.-C., Dorale, J.A., 2001. A high-resolution absolute-dated late Pleistocene monsoon record from Hulu Cave, China. Science 294, 2345–2348.
Wang, Y.-J., Cheng, H., Edwards, R.L., Kong, X., Shao, X., Chen, S., Wu, J.Y., Jiang, X., Wang, X., An, Z.S., 2008. Millennial- and orbital-scale changes in the East Asian monsoon over the past 224,000 years. Nature 451, 1090–1093.